On Water Flow in Hot Fractured Rock —

A Sensitivity Study on the Impact of Fracture-Matrix Heat Transfer

Jens T. Birkholzer and Yingqi Zhang

Ernest Orlando Lawrence Berkeley National Laboratory,
1 Cyclotron Road, MS 90-1116, Berkeley CA 94720
Fax: (510) 486-5686; Email: jtbirkholzer@lbl.gov

Abstract

Dual-continuum models have been widely used in modeling flow and transport in fractured porous rocks. Among many other applications, dual-continuum approaches were utilized in predictive models of the thermal-hydrological conditions near emplacement tunnels (drifts) at Yucca Mountain, Nevada, the proposed site for a radioactive waste repository in the U.S. In unsaturated formations such as those at Yucca Mountain, the magnitude of mass and heat exchange between the two continua—fracture network and matrix—is largely dependent on the flow characteristics in the fractures, because channelized finger-type flow strongly reduces the interface area between the matrix surfaces and the flowing liquid. This effect may have important implications, for example, during the time period that the fractured rock near the repository drifts would be heated above the boiling point of water. Depending on the magnitude of heat transfer from the matrix, water percolating down the fractures will either boil off in the hot rock region above drifts or may penetrate all the way to the drift walls and possibly seep into the open cavities. In this paper, we describe a sensitivity analysis using a variety of approaches to treat fracture-matrix interaction in a three-dimensional dual-continuum setting. Our simulation example is a laboratory heater experiment described in the literature that provides evidence of rapid water flow in fractures, leading to drift seepage despite above-boiling conditions in the adjacent fractured rock. The experimental finding can only be reproduced when the interface area for heat transfer between the matrix and fracture continua is reduced to account for flow channeling.

1. Introduction

Analysis of the proposed underground repository for high-level radioactive waste at Yucca Mountain, Nevada, requires knowledge of water flow in the unsaturated fractured rock at strongly elevated temperatures caused by heat emanating from the decaying waste. If infiltrating water penetrates through the hot rock regions above the repository and seeps into the emplacement tunnels (drifts), it can promote the corrosion of waste packages and enhance the release of radionuclides. Since the liquid water, which is mostly flowing in the well-connected rock fractures, will be subject to effective vaporization from the adjacent rock matrix, the hot (at above-boiling temperature) rock zone forming above the repository may significantly reduce the possibility of water contacting waste packages (Ramspott, 1991; Wilder, 1993; Buscheck and Nitao, 1993).

The thermal-hydrological (TH) conditions in the unsaturated environment at Yucca Mountain following waste emplacement have been evaluated in various modeling studies (e.g., Pruess et al., 1990a, b; Pruess and Tsang, 1993, 1994; Haukwa et al., 1999; Buscheck et al., 2002). Most of these studies use some form of dual-continuum approach that separately describes the TH conditions in the fractures and the rock matrix because of their strongly different properties. It was generally demonstrated that, according to current design options, a large dry rock region would exist at above-boiling temperatures in the vicinity of waste emplacement drifts for hundreds of years. The heated rock is expected to form an effective vaporization barrier, which would prevent percolating water from arriving at the drift walls (BECHTEL SAIC COMPANY, 2004a; Birkholzer et al., 2004). Thus, thermal seepage of water into drifts should not be of concern during the "hot" phase of the repository. (In the context of this paper, thermal seepage is defined as seepage of water into drifts despite above-boiling average temperatures in the near-drift fractured rock.) *In situ* heater experiments conducted at Yucca Mountain have demonstrated that (a) a good agreement between measured data and simulation results can be achieved, and (b) conditions at the drift walls are essentially dry; they show no indication of local breaching of the vaporization barrier (Tsang and Birkholzer, 1999; Birkholzer and Tsang, 2000; Mukhopadhyay and Tsang, 2002; Mukhopadhyay and Tsang, 2003).

Recent experimental results, however, may pose a challenge to the conclusions about thermal seepage at Yucca Mountain, suggesting that the exclusion of liquid water from hot rocks may not be complete. A laboratory heater test conducted by the Center for Nuclear Waste Regulatory Analyses at the Southwest Research Institute in San Antonio (hereafter referred to as the

CNWRA experiment) indicated that water rapidly flowing in vertical fractures was able to penetrate into a above-boiling rock region and seep into a horizontal cylindrical opening (Green and Prikryl, 1998, 1999; Green et al., 2003). In other words, thermal seepage was shown to be possible. In contrast to the *in situ* heater tests at Yucca Mountain, where natural percolation is relatively small, the CNWRA experiment was operated using artificial water release from the top of the experimental apparatus, testing the thermal seepage potential for rather extreme flow conditions.

The question arises whether the simulation models used for predicting TH conditions at Yucca Mountain would be capable of explaining the observation of thermal seepage in the CNWRA experiment. One concern about these models is the use of continuum approaches, which generally involve some sort of averaging and homogenization of heterogeneous formation properties, and tend to underestimate the probability of small-scale processes, such as formation of channelized, finger-type flow paths. As a result, the amount of heat available to vaporize the water flowing in fractures may be overestimated, because the full geometric contact area is used for energy transfer from the adjacent hot rock matrix rather than the area where the flow actually occurs. In general, rapid channelized flow events are more likely to overcome the vaporization barrier (Pruess and Tsang, 1994). This possibility was demonstrated, for example, using analytical (Phillips, 1996) and semi-analytical solutions (Birkholzer, 2003; Birkholzer and Ho, 2003; Birkholzer et al., 2003) that investigate the fate of discrete finger-type flow events penetrating a vertical fracture surrounded by a hot rock matrix. Since these solutions use various geometric and conceptual simplifications, they are mostly limited to conceptual studies and cannot be used for the complex modeling applications necessary for predicting Yucca Mountain's future TH conditions.

Regarding isothermal flow and transport, various researchers have improved classic dual-continuum approaches to account for channelized flow in fractures and the related reduction in fracture-matrix (F-M) mass transfer. The improved approaches adjust the interface area between fractures and matrix, depending on the flow characteristics in the fractures. The adjusted interface area represents the fraction of the full geometric interface that actively participates in fluid and solute exchange (e.g., Ho, 1997; Bandurraga and Bodvarsson, 1999; Doughty, 1999; Liu et al., 1998; Liu et al., 2003). In the unsaturated zone at Yucca Mountain, this "active" fraction is often much smaller than the full interface, because many of the fractures are not contributing to flow, and because flow through fracture planes may be highly channelized. Various approximate formulations were proposed for F-M interface reduction, including, for example, multiplication

with a constant factor, with a power function of fracture liquid saturation, or with fracture relative permeability, all summarized and systematically tested in Doughty (1999), as well as multiplication with a factor derived from the more recent active fracture model developed by Liu et al. (1998).

Significantly less research work regarding interface reduction approaches was conducted for heat transfer problems, possibly because the concept of channelized fracture flow in heated rocks involves a local thermodynamic disequilibrium between the liquid and the gas phase in the fractures, a conceptual challenge for most multiphase simulators. In prior work (Birkholzer et al., 2004), we introduced the so-called thermal seepage model, a dual-continuum model specifically designed to evaluate the potential of drift seepage during the heating phase of the Yucca Mountain repository. As a conservative choice, the model utilizes a small factor reducing the amount of heat transferred between heated matrix blocks and fracture water (Bechtel SAIC Company, 2004a). Predictive simulation suggested that, for the conditions at Yucca Mountain, channelized flow is not likely to result in seepage during the time that the matrix temperature is above boiling, because water is unable to penetrate far into the hot rock despite the strongly reduced F-M interface area.

The objective of this work is to improve our understanding of thermal seepage by evaluating the applicability and impact of F-M interface reductions in heat-transfer problems. We adopt the general modeling concept of the thermal seepage model (Birkholzer et al., 2004), apply different F-M area formulations known from ambient flow and transport studies, and test the sensitivity of the TH conditions to these formulation choices. The sensitivity study is conducted using the CNWRA experiment as a simulation example. Our goal is (1) to demonstrate that the thermal seepage model is capable of explaining the thermal seepage observations from the laboratory experiment, (2) to identify the F-M area formulation best suited for this purpose, and (3) to evaluate whether the test conditions and observations in the CNWRA experiment are representative of the TH conditions expected at Yucca Mountain.

2. Basic Processes and Modeling Concepts

2.1 Thermal-Hydrological Processes in Fractured Porous Rock at Yucca Mountain

The fractured tuff in the hydrogeological units hosting the proposed repository at Yucca Mountain is characterized by strong intrinsic heterogeneity. The tuff matrix has a rather large porosity between 0.1 and 0.2, but a very small permeability (on the order of microdarcies). On the other hand, the formation is intensely fractured, with fracture spacings of a few decimeters or less, and the continuum permeability of the fractures is many orders of magnitude larger than that of the rock matrix. Since the fractures occupy only a very small volume fraction of the formation, the porous matrix stores the vast majority of the mass and energy in the system and accounts for most of the heat conduction. Initially, before the start of heating, the matrix pores are about 80 to 90% saturated with water, whereas the fractures are essentially dry (Birkholzer and Tsang, 2000).

The heat generated by the decaying radioactive waste at Yucca Mountain will induce strong TH processes in the fractured rock, which are schematically illustrated in Figure 1 (Birkholzer et al., 2004). After emplacement of the waste, heat is transferred from the waste packages to the drift walls and subsequently migrates radially outward, mostly by conduction in the matrix. As temperatures in the fractured rock exceed the boiling point of water, the stagnant water in the matrix pores becomes mobile by vaporization. Most of the vapor moves away from the vicinity of the drift through the permeable fracture network. With continuous heating, a hot dryout zone will develop near the drifts, while condensation of vapor occurs in the fractures further away from the heat source. Condensation above the heated areas may result in gravity-driven flow of water back toward the heated drift. Whether refluxing condensate boils off in the dryout zone or is able to reach the drift wall depends on the extent of the vaporization zone, the intensity of heating, and the small-scale flow characteristics. As mentioned before, water is more likely to penetrate into the hot dryout zone if the condensate reflux occurs in the form of channelized, finger-type flow. Water that reaches the drift wall may or may not seep into the open drift, depending on the effectiveness of capillary forces at the rock-drift interface that tend to keep water in the formation (e.g., Finsterle et al., 2003; Ghezzehei et al., 2004).

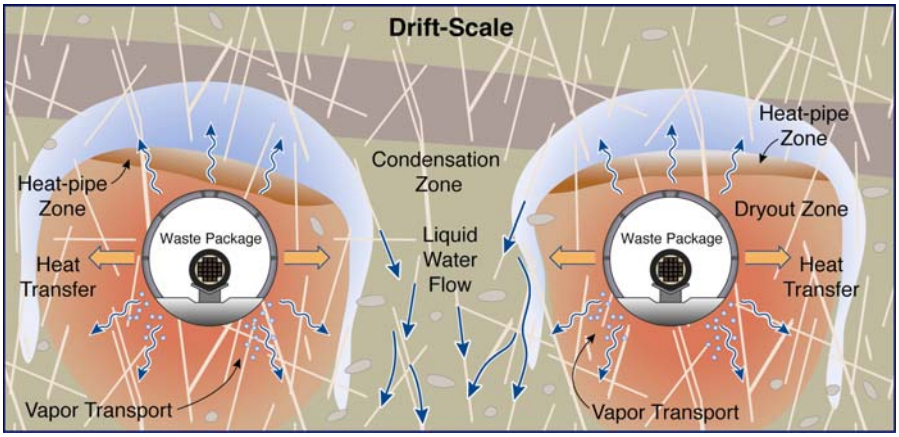

Figure 1. Schematic of expected TH conditions near emplacement drift at Yucca Mountain (not to scale)

2.2 Brief Description of the Thermal Seepage Model

The thermal seepage model is a drift-scale, dual-continuum process model developed by Birkholzer et al. (2004) to evaluate the evolution of drift seepage over the time period relevant for the repository at Yucca Mountain. This period comprises short-term hot conditions, when the exclusion of formation water from emplacement drifts is mostly dependent on vaporization, as well as long-term "back-to-ambient" conditions, when capillary forces at the drift wall limit water entry into drifts. The goal of the modeling effort was to examine whether or not thermal seepage could occur at Yucca Mountain considering the possibility of strongly channelized flow in the fractures. The model combines the conceptual framework used in previous drift-scale TH models for Yucca Mountain (Birkholzer and Tsang, 2000; Haukwa et al., 2003) with modeling elements developed for ambient seepage studies, in which capillary forces at the rock-drift interface are relevant (Finsterle et al., 2003; Ghezzehei et al., 2004). While the details of the model are given in Birkholzer et al. (2004) and Bechtel SAIC Company (2004a), the main model elements are listed below for convenience:

- Small-scale heterogeneity of fracture permeability is represented in the model as an important factor promoting channelized flow and local saturation buildup, both of which affect ambient as well as thermal seepage (Birkholzer et al., 1999; Birkholzer et al., 2004).
- A specific boundary condition is implemented for the capillary barrier behavior of the fracture continuum at the rock-drift interface, developed based on measured seepage rates obtained in liquid-release tests (Finsterle et al., 2003; Ghezzehei et al., 2004).

- F-M interface reduction is accounted for in the model for both liquid and heat transfer processes. In order to be conservative (i.e., to arrive at upper-bound predictions for thermal seepage), heat transfer is reduced using a very small interface reduction factor of about 0.002 (Bechtel SAIC Company, 2004[1]). Such conservatism was deemed adequate because of the large uncertainties related to channelized flow and thermal interaction between fractures and matrix. The conceptual framework for heat-exchange reduction between fractures and matrix is further discussed in Section 2.3.

The TH simulations were conducted using TOUGH2 (Pruess et al., 1999), a simulator for coupled fluid and heat flow of multiphase, multicomponent fluid mixtures in porous and fractured media. TOUGH2 assumes local thermodynamic equilibrium in each computational cell.

2.3 Fracture-Matrix Interaction Models for Heat Transfer

Consider isothermal finger-type flow along an unsaturated fracture next to a porous matrix block (Figure 2). As the fingers migrate, part of the water imbibes into the matrix pores as a result of capillary force differences. However, imbibition is only active over the wetted fraction of the fracture surface. In contrast, the exchange of gas between the fractures and the matrix, a possible result of gas pressure differences, occurs only over the nonwetted fracture surface. It is obvious that these characteristics of pore-scale channeling processes affect the magnitude of fracture-matrix interaction, and that the F-M interface area to be used for the calculation of liquid or gas flow between fractures and matrix is generally smaller than the full geometric interface (Ho, 1997; Liu et al., 1998).

Let us now assume that the matrix block is heated to an average temperature T_M, and that the liquid fingers represent the gravity-driven flow of relatively cool water (temperature $T_{F,L}$) down the hot fracture surface. If the downward flow is fast, the conductive heat provided by the matrix will not be sufficient to immediately raise the water temperature to that of the matrix rock. As a result, a local thermodynamic disequilibrium is to be expected, not only between the liquid finger and the adjacent rock matrix, but also between the water phase and the gas phase in the fracture. (The gas phase in the fractures remains largely in equilibrium with the matrix; i.e., the gas temperature, $T_{F,G}$, is always close to the average matrix temperature, T_M). In case the matrix

[1] Instead of modifying the actual interface area, the F-M heat transfer reduction was realized in the thermal seepage model by an equivalent adjustment of the thermal conductivity used for the heat exchange between the fractures and the matrix (BSC, 2004).

temperature is above boiling, water in the flow channels will vaporize as it migrates downward. The more focused the channelized flow, the smaller the interface area available for heat flow from the matrix to the liquid water, and the farther the penetration of liquid water into the hot fracture until vaporization is complete (Birkholzer, 2002).

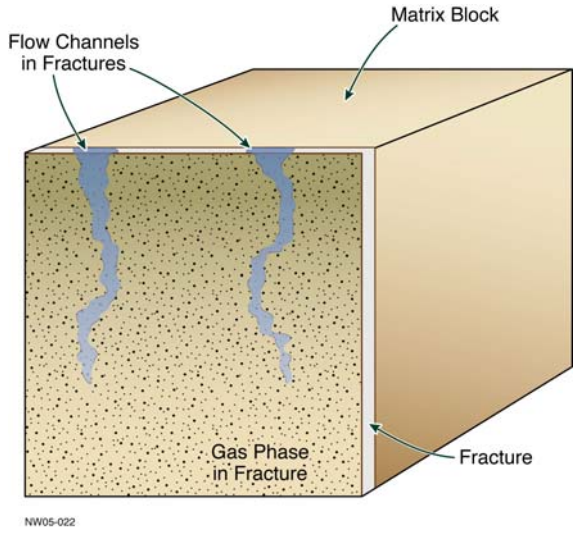

Figure 2. Schematic illustration of channelized flow in a fracture-matrix system

In dual-continuum models such as those employed in this study, the small-scale flow and transport processes shown in Figure 2 are represented by well-known effective-continuum concepts, formulated separately for the fractures and the matrix blocks (Pinder et al., 1993). In general, continuum concepts for two-phase flow of water and air in gaseous and liquid phases use saturations to describe the relative fraction of each phase in the pore space. Darcy's law is applied to the gas- and liquid-phase flows separately (e.g., Pruess, 1987, 1999), with characteristic functions (e.g., van Genuchten, 1980) used to describe the interference between the phases dependant on the saturation values. The F-M interaction of gases and liquids can be described by such concepts in a straightforward manner, calculating the flow rates as a function of the state variables and properties associated with the porous fractured medium (Ho, 1997). For example, the flow rate of liquid water from the fracture continuum to the matrix continuum can be written as follows (e.g., Liu et al., 1998):

$$F_L = K_L(S_L) A_{FM} \frac{P_{cF}(S_L) - P_{cM}(S_L)}{d} R_L \ , \qquad (1)$$

where $K_L(S_L)$ is the unsaturated hydraulic conductivity for liquid water between a fracture element and the corresponding matrix element, A_{FM} is the geometric area between all fractures

and matrix blocks lumped into a computational element, $P_{cF}(S_L)$ and $P_{cM}(S_L)$ are capillary pressures of fracture and matrix elements, respectively, and d is a representative distance between the fracture and matrix block centers. Finally, R_L denotes the interface reduction factor for liquid flow, which accounts for the impact of fingering or non-active fractures on the effectiveness of F-M interaction. Note that expressions similar to Equation (1) can be written for the gas flow between the two continua, using an interface reduction factor for gas flow, R_G. However, the interface reduction for gas flow is often neglected in unsaturated media problems because its effect is typically small (Doughty, 1999).

As mentioned before, different formulations for R_L have been proposed in the literature, including a constant factor, a power function of liquid saturation, or the liquid-phase relative permeability (Altman et al., 1996; Ho, 1997; Doughty, 1999). In the first formulation, the constant multiplier is typically treated as a fitting parameter to be determined from comparison with measured data. The other two formulations include some functional dependence on the saturation in the fractures to accommodate changes in the hydraulic state, which is physically more meaningful than the constant factor approach.

A rigorous method for deriving R_L was later developed by Liu et al. (1998), based on the hypothesis that the interface reduction factor (as well as the characteristic functions for unsaturated flow) should be based on the fraction of so-called active fractures. Active fractures are defined as those fractures or portions of fractures that actively conduct water at a given hydraulic state. Liu et al. (1998) suggested expressing the active fraction as a power function of water saturation, with the power function coefficient γ a positive constant depending on properties of the corresponding fracture network. It follows from the active fracture concept that the effective saturation of active fractures, $S_{Le,a,}$ is larger than the effective saturation of all connected (but partially inactive) fractures, S_{Le}. Based on activity of the fracture network, Liu et al. (1998) developed a consistent mathematical framework for (1) modifications to the F-M interface area and (2) modifications to the characteristic functions for unsaturated flow. Following Liu et al. (1999), the F-M interface reduction factor in active fracture models can be derived as follows:

$$R_L = S_{Le}^{1+\gamma} = S_{Le,a}^{\left(\frac{1+\gamma}{1-\gamma}\right)} \quad . \tag{2}$$

Note that $\gamma = 0$ corresponds to the case where all connected fractures are actively conducting flow. In this case, $R_L = S_{Le} = S_{Le,a}$, i.e., the interface reduction factor is equal to the effective saturation.

In principle, the dual-continuum formulation for heat flow should follow a methodology similar to that developed for liquid and gas flows. For example, in correspondence to Equation (1), the heat transferred from the hot matrix to the cooler liquid water flowing in fractures should be expressed as

$$F_{H,L} = \lambda \, A_{FM} \frac{T_M - T_{F,L}}{d} R_{H,L} \, , \tag{3}$$

where λ is thermal conductivity and $R_{H,L}$ is the interface reduction factor for heat exchange between the matrix and the water in the fractures. Assuming that this factor is mostly governed by flow geometry considerations (i.e., fracture network characteristics, activity of fractures, finger flow), the reduction factor derived for liquid exchange, R_L, should be identical to the reduction factor derived for heat exchange, $R_{H,L}$. However, Liu et al. (1998) acknowledge that F-M interaction can also be affected by fracture coatings (Thoma et al., 1992), which could have a different impact on liquid versus heat transfer across the interface. Also, at above-boiling conditions, vapor films may evolve between the flowing water body and the fracture wall, potentially changing the heat-transfer conditions. Thus, there is a possibility that $R_{H,L}$ may be different from R_L. One may safely assume, however, that the different interface-reduction formulations developed and applied to liquid and gas flows should also provide reasonable choices for heat exchange.

While heat is transferred from the rock matrix to the liquid phase in the fractures according to Equation (3), there is a simultaneous heat transfer between the rock matrix and the gas phase in the fractures, which can be written as

$$F_{H,G} = \lambda \, A_{FM} \frac{T_M - T_{F,G}}{d} R_{H,G} \, . \tag{4}$$

Here, $R_{H,G}$ is the interface reduction factor for heat exchange between the matrix and the gas in the fractures. Remember that for rapid finger flow into an initially hot fractured rock system, the liquid temperature in the fracture continuum may be much cooler than the temperature in the

adjacent matrix, while the gas temperature is usually fairly well equilibrated with the matrix temperature. Thus, rigorously applying Equations (3) and (4) in a numerical simulation would involve allowing for a disequilibrium between the phase temperatures in each computational grid-block, a condition that cannot be captured by the local thermal equilibrium assumption of most multiphase, multicomponent simulators. (TOUGH2, as an example, allows for local disequilibrium between the fracture and the matrix continua via its dual-continuum capabilities, but cannot account for local disequilibrium between the water and the gas phase.)

This conceptual difficulty explains why the necessity of reducing the F-M interface area in response to the hydraulic state of fracture flow is largely ignored when considering non-isothermal conditions. For example, Ho (1997) and Doughty (1999) conducted systematic evaluation of various F-M interface reduction approaches for moisture and gas transport, but both opted to assume a full geometric interface area for heat transfer between the rock matrix and the fractures. The latter is equivalent to assuming that the water and gas phases are well mixed and uniformly distributed over the geometric fracture area, and that the two phases are always in local thermal equilibrium. Doughty (1999) acknowledges that this simplified treatment was chosen not because it was considered physically rigorous, but "due to the complexity of the problem." Green et al. (2003) and Birkholzer et al. (2004) used constant-factor reductions for heat-transfer problems, but did not indicate whether the reduction was deemed necessary because of flow channeling in the fractures. Other factors—such as fracture coatings, vapor films, or initial overestimation of the geometric interface—would also require reduction in heat transfer between fractures and matrix, but would not cause a local disequilibrium between gas and liquid phases.

In this paper, we introduce a rigorous conceptual framework for dual-continuum modeling of TH processes in hot fractured rock with (1) flow channeling in fractures, (2) interface reduction in F-M heat transfer, and (3) local disequilibrium between gas and liquid phases. We suggest an approximate solution that allows the use of local-equilibrium simulators such as TOUGH2, based on the assessment that an accurate representation of the gas-phase temperature in the fractures is not necessary. Therefore, it is possible to use Equation (3) for the heat transfer between the matrix and the liquid phase, while ignoring the heat transfer between the matrix and the gas phase in Equation (4). Both phases in the fractures are then represented by the liquid-phase temperature, thereby avoiding the necessity of simulating disequilibrium phase temperatures. While this approximation accurately accounts for the limited heat exchange between the rock matrix and the liquid water in the fractures, it misrepresents the gas-phase temperature in the fracture. We shall demonstrate in the Appendix that this misrepresentation has a minor impact on the TH conditions

in the fractured rock because of (1) the small relative error in energy storage, and (2) the small relative error in interphase heat transfer. The proposed method allows using any of the interface reduction formulations developed for liquid transfer processes.

3. The CNWRA Heater Experiment

The CNWRA experiment (Green and Prikryl, 1998, 1999; Green et al., 2003) was conducted to assess the TH conditions around a heat source in a fractured porous formation with gravity-driven water flux from above. A 1.2 x 0.6 x 1.2 m^3 test cell was assembled using solid rectangular concrete blocks (0.05 x 0.6 x 0.05 m^3) (see Figure 3a) with measured TH property values. The concrete blocks, made from a mixture of bentonite clay, barite, and portland cement, were placed into a loading frame so that compressive stress could be applied. The spaces between the blocks (estimated at about 400 micron aperture) represented two sets of horizontal and vertical fractures. Because of the arrangement of the concrete slabs, the fracture sets within the test were regularly structured and continuous. The assembly of concrete blocks formed a “fracture-matrix” system with a permeable fracture network next to low-permeability, porous “matrix blocks.”

The apparatus was insulated with neoprene and styrofoam layers to reduce heat and mass losses. A 0.15 m diameter borehole of 0.6 m length was drilled into the center of the test cell to simulate a drift. A 0.15 m long, 0.019 m diameter cylindrical heater was placed into the middle section along the drift, arranged on a small pedestal approximately 0.015 m above the floor. A maximum power of 142 W was applied, enough heat to ensure boiling conditions in the vicinity of the drift. To simulate water release from above, tap water from a carbonate aquifer was introduced at a rate of 1,000 mL/day (approximately one drop per second) into a centrally located 0.3 m long cylinder at the top of the test cell, and was allowed to infiltrate downward toward the heat source. This setup was intended to represent the possible gravity-driven flux of water above heated drifts at Yucca Mountain, stemming from percolating water as well as from condensation of vaporized pore water. Note, however, that the central vertical fracture in the CNWRA experiment provides a direct flow path from the water release point to the crown of the drift.

Three different thermal experiments were conducted that essentially differed by the duration of heating and water release. The first test ran for 50 days (Green and Prikryl, 1998), the second for 140 days (Green and Prikryl, 1999; Green et al., 2003), and the third for 215 days (Green et al., 2003). In this paper, the second experiment is evaluated, which started with 5 days of heating without water release, followed by 125 days of heating and infiltration, and completed by 10 days

of infiltration during linear ramp-down of the heat source. We refer to the first 130 days of the experiment as the heating phase and the final 10 days of the experiment as the cooling phase.

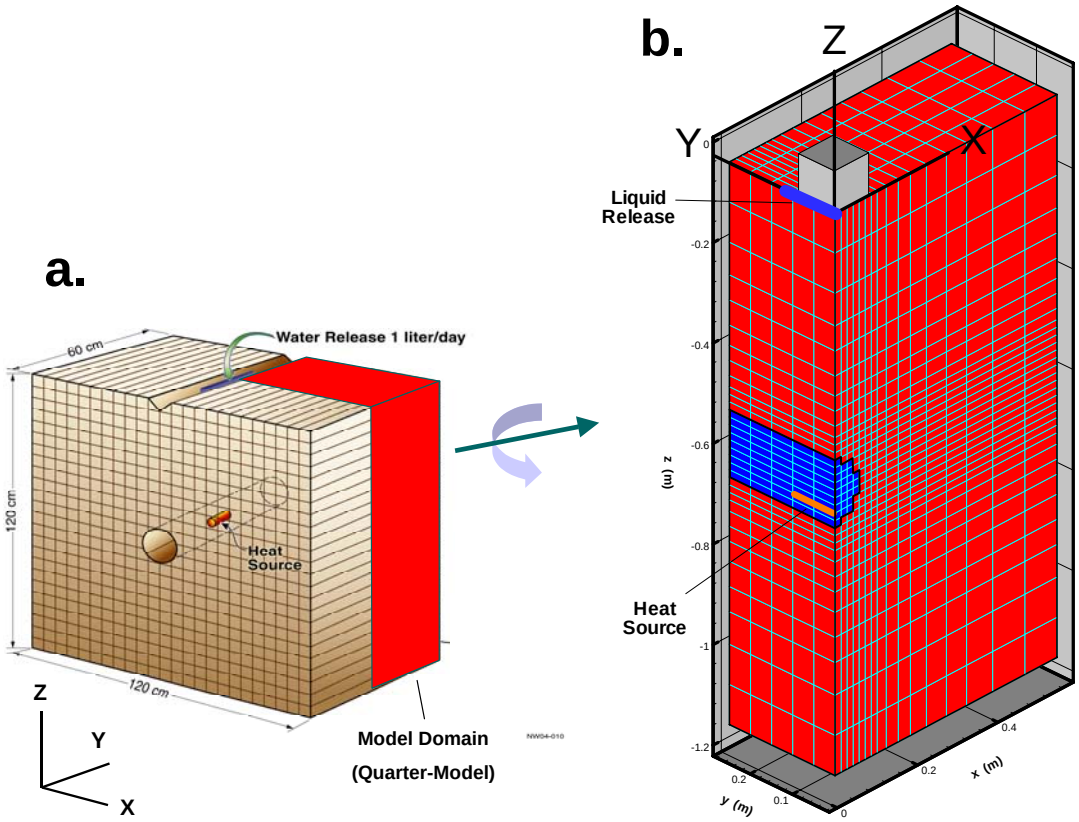

Figure 3. Schematic of (a) CNWRA heater experiment and (b) simulation domain with finite volume grid. The simulation domain—reduced to one quarter of the laboratory test cell—is rotated around the Z-axis to allow for better visualization. The local coordinate system of the simulation domain is located at the top of the test cell in the center of the liquid-release cylinder. The Y-axis is aligned with the drift axis.

During the experiment, gas pressure and relative humidity were measured within the drift. Temperature was recorded with about 100 thermocouples, many of which were placed into the central vertical fracture that directly connects the water-release location with the drift crown. Within the fractured medium, a maximum temperature of 202ºC was reported at a distance of 0.0125 m into a fracture immediately below the heater (Green and Prikryl, 1999). Above the heater, a maximum temperature of 175ºC was measured at the drift surface in the center cell of the drift crown.

Thermocouples in the central fracture indicated the location of the boiling point isotherm (i.e., about 100°C) at about 10 cm above the drift crown at early stages (after ten days of heating and 5

days of infiltration). With continuing infiltration, the boiling isotherm migrated downward to roughly 5 cm above the drift crown. No fluctuations were detected in these temperature measurements, which would have indicated the presence of fast, downward moving water temporarily depressing the reading. However, Green and Prikryl (1999) acknowledge that the spatial and temporal resolution of the temperature measurements was rather coarse, and that narrow, possibly episodic ribbons of water may have penetrated the boiling zone toward the heater without being detected by sensors. Analysis of precipitates deposited in the borehole indicated that some water must have advanced toward the heater and dripped into the drift during the heating phase of the experiment, indicating that both vaporization and capillary barriers had failed. It was concluded from the experiment that the presence of a hot dryout zone in the fractured rock did not preclude the dripping of water into a heated drift, a process that could lead to accelerated waste-package corrosion if occurring in Yucca Mountain drifts.

4. Simulation of the CNWRA Experiment

In this section, we apply the general modeling concept of the thermal seepage model (Section 2.2) to the CNWRA experiment. This allows us to evaluate the modeling framework for a test case in which the barrier capabilities of heated fractured rock are challenged by significant water drainage from above. The test cell is represented as a dual-continuum system, with a matrix continuum for the concrete blocks and a fracture continuum for the gaps between them. The heat transfer between fractures and matrix is treated following the new conceptual framework proposed in Section 2.3, and different F-M area formulations are applied to understand the related sensitivities. For comparison, we also conduct simulation runs where the full geometric interface area is available for F-M heat transfer. The open borehole in the test cell is modeled as a single, gas-filled, highly permeable continuum, with an equivalent thermal conductivity accounting for the effect of radiative and convective heat exchange within the borehole.

In contrast to the thermal seepage model for Yucca Mountain (Birkholzer et al., 2004), we did not attempt to actually predict drift seepage by explicitly simulating the capillary barrier at the drift wall. As pointed out in Finsterle et al. (2003), reliable seepage predictions require calibration of the model to measured seepage rates, which are not available in the CNWRA experiment. Instead, we model the drift wall as a fully effective capillary barrier and conduct a qualitative assessment of thermal seepage potential based on the simulated water accumulation in the fracture continuum immediately above the heated drift. It was shown in ambient seepage modeling studies for Yucca Mountain (e.g., Finsterle et al., 2003; Ghezzehei et al., 2004) that

seepage may commence for fracture continuum saturations at the drift wall that are much smaller than unity (i.e., much smaller than full saturation). In these models, a specific seepage boundary condition at the drift wall accounts for seepage-promoting factors that cannot be explicitly captured in a continuum model. One of these factors is the possible presence of discrete fracture segments intersected by the drift opening. If these segments do not extend far enough laterally or do not have a lateral connection to other fractures, the water carried in these segments cannot bypass the opening. (Notice that this situation exists in the CNWRA experiment, where vertical fracture segments immediately above the drift have no lateral connection.) Another important factor are small-scale heterogeneities in fracture permeability, which can create local ponding conditions at the drift wall. Our CNWRA simulation model does not account for such small-scale heterogeneity, because the necessary input data from small-scale permeability measurements were not available in the experiment.

Let us discuss at this point whether the choice of a continuum model, one of the key features of the thermal seepage model, is adequate for the considered problem. At Yucca Mountain, adequacy of the continuum concept is based on the considerable density of the natural fracture network, which is well connected on a scale much smaller than a typical emplacement drift, i.e., the geometry of interest for seepage. Comparison of modeling results with *in situ* experiments at Yucca Mountain has demonstrated that the relevant physical processes in the near-drift fractured rock, both ambient and thermal, are well captured on that scale (e.g., Finsterle et al., 2003 for ambient processes; Birkholzer and Tsang, 2000 for thermal processes). The fracture geometry in the CNWRA experiment is rather artificial, with continuous fractures and equal fracture spacing. In general, these characteristics are well suited for an effective continuum representation. On the other hand, because of the small distance between water release and borehole and the small borehole diameter compared to the fracture spacing, the experiment results may be dominated by a few vertical and horizontal fractures, therefore suggesting that a discrete representation of these dominant features may be appropriate.

Our main focus in this paper is to understand the importance of F-M heat transfer concepts in evaluating heat transfer problems in fractured porous rock. We furthermore seek to demonstrate that an established modeling methodology, based on a dual-continuum representation of the fractured rock, is capable of reproducing the main findings of the laboratory experiment. It is not the aim of this paper to simulate the CNWRA experiment in all its qualitative and quantitative detail. We therefore employ a continuum model rather than a discrete fracture model, aware of the limitations of this modeling approach. Continuum representations of the CNWRA experiment

were also employed in the complementary modeling studies of Green and Prikryl (1999) and Green et al. (2003).

4.1 Model Setup, Boundary Conditions and TH Properties

The CRWRA experiment is simulated in a three-dimensional model domain. Symmetry along two vertical planes justifies a model domain reduced to one-quarter of the laboratory test cell. The one-quarter model and the numerical discretization used for the dual-continuum grid are shown in Figure 3b. The grid consists of about 7,800 grid elements.

Most of the test conditions and properties used in our simulation model are directly based on the literature describing the experiment and related analyses (Green and Prikryl, 1998, 1999; Green et al., 2003). Initially, the test cell is assumed to be dry at a gas pressure of 1 bar and a temperature of 20^{o}C. (We assume dry conditions because most of the water in concrete is chemically bonded due to hydration, and is thus not available for flow and vaporization.) The transient simulation runs over the 140 days of heating in the experiment. As heating starts, one quarter of the total power of 142 W is introduced in grid elements representing the heat source. At 5 days of heating, water is released into fracture-continuum elements that represent the release cylinder at the top of the model domain. Starting at 130 days of heating, the thermal energy is linearly scaled down over the remaining 10 days of the experiment. Conductive heat loss is considered by explicitly modeling the insulation layer around the test cell, with the thermal properties of the insulation material estimated from qualitative comparison of temperature results with reported measurements. To allow for gas release, the boundary elements were assigned a small gas permeability of 10^{-15} m^2. Liquid flow across the boundaries is not permitted, consistent with Green et al. (2003).

The thermal-hydrological properties assigned to the fracture and matrix continua are given in Table 1. Uniform properties are used throughout the test cell. All relevant material properties for the concrete matrix are taken from measurements (Green et al., 2003), with the exception of matrix permeability, which was reduced by one order of magnitude compared to the measured value. Green et al. (2003) suggested that such a reduction in matrix permeability could better reproduce observed matrix saturation patterns. Since direct measurements are not available, fracture properties are mostly estimated, based on (1) the known fracture geometry, (2) estimates of the average geometric fracture aperture (0.4 mm as reported in Green and Prikryl (1998)), and (3) literature data from similar settings. Note that fracture continuum permeability is anisotropic in our model, since both fracture sets (vertical and horizontal) conduct in the y-direction (i.e.,

parallel to the borehole axis), but only one fracture set conducts in the x- and z-directions, respectively. The permeability values are calculated from a parallel-plate assumption using the geometric aperture of 0.4 mm, but were reduced by one order of magnitude to correct for hydraulic aperture being smaller than geometric aperture. Fracture capillarity is directly based on capillary theory for a parallel-plate conduit of 0.4 mm aperture. Overall, the properties listed in Table 1 are similar to those used in Green et al. (2003).

Table 1. Hydrogeological and thermal input values for simulation model

Parameter	Value
Material Properties	
Matrix Permeability	2×10^{-18} m^2
Matrix Porosity	0.5
Matrix Grain Density	1600 kg/m^3
Matrix Grain Heat Capacity	840 J/kg/K
Matrix Dry Thermal Conductivity	0.5 W/m/K
Matrix Wet Thermal Conductivity	1.0 W/m/K
Fracture Permeability (y-direction)	2.12×10^{-11} m^2
Fracture Permeability (x- and z-direction)	1.06×10^{-11} m^2
Fracture-Matrix Geometry Assumed for Dual-Continuum Formulation	
Volume Fraction of Fractures	0.016
Fracture-Matrix Interface Area	3.76 m^2 per unit volume of rock
Representative Distance between Fracture and Matrix Block	0.00625 m
Characteristic Curves	
Matrix Residual Liquid Saturation	0.01
Matrix Van Genuchten Parameter, α	6.36×10^{-7} 1/Pa
Matrix Van Genuchten Parameter, m	0.37
Fracture Residual Liquid Saturation	0.01
Fracture Van Genuchten Parameter, α	2.9×10^{-3} 1/Pa
Fracture Van Genuchten Parameter, m	0.8

Note: The characteristic curves utilize the functional forms introduced by van Genuchten (1980), with a slight modification regarding the maximum possible capillary pressure at small saturations. Following Liu et al. (1998), the same characteristic curves are used for the active fracture model, but saturation of all fractures is replaced by saturation of active fractures. The saturation-dependent thermal conductivity in the matrix is interpolated between dry thermal conductivity (oven-dried sample) and wet thermal conductivity (water-saturated samples) as a square-root function of saturation. The representative distance between fracture and matrix blocks to be used in dual-continuum formulations is estimated from the fracture network geometry following Pruess (1983), who suggested a representative distance of $d = D/8$ for a two-dimensional fracture network (i.e., two fracture sets) with uniform fracture spacing D.

Dual-continuum models require information on the respective volume fractions of fractures and matrix blocks in the domain, the geometric interface area between fractures and matrix blocks, and the average distance from a typical matrix block center to the adjacent fractures. For the regular geometry in the CNWRA experiment, these properties were directly derived from geometric considerations.

4.2 Model Results

Modeling of the CNWRA experiment was conducted using TOUGH2 (Pruess et al., 1999), with some modifications made to incorporate interface reduction formulations for heat exchange between the fractures and matrix. Section 4.2.1 below gives an overview of the interface reduction formulations evaluated in this study. Note that our sensitivity cases account for the reduced transfer of liquid and heat between fractures and matrix, but, following Doughty (1999), always assume a full geometric interface for gas flow.

4.2.1 Simulation Cases

Table 2 summarizes the sensitivity cases analyzed in this paper. Our focus is on understanding sensitivity to F-M heat transfer; thus, our cases differ in the treatment of interface-area reduction between fracture and matrix continua. The sensitivity cases include interface reduction by (a) multiplication with fracture saturation, (b) multiplication with constant factors of 0.1, 0.01, and 0.002, and (c) reduction factors based on the active fracture model with γ values of 0.3 and 0.569. To differentiate between the impact of liquid and heat transfer approaches, we simulate each interface reduction case in two different ways. First, we conduct a simulation reducing the interface area for liquid transfer between fractures and matrix, but not for heat. Second, we conduct a simulation reducing the interface area for liquid *and* heat transfer, following the approach outlined in Section 2.3. For comparison, we also conduct a simulation with a full geometric interface, hereafter referred to as Case F.

We have plotted the resulting interface reduction factors as a function of saturation in Figure 4. For cases using the active fracture model, we display the saturation of active fractures, $S_{Le,a}$. As shown in Table 2, the maximum fracture saturations simulated in the CNWRA experiment are typically less than 0.2 (in some cases up to 0.3), which defines the saturation range displayed in Figure 4. Some cases are associated with a significant reduction in the geometric interface, most notably the constant-factor case with 0.002 and the active fracture case with γ = 0.569. The smaller the interface area, the more likely the fast flow of water from the injection point down to

the heated borehole. For active fracture modeling at Yucca Mountain, Liu et al. (2003) derived γ values between 0.2 and 0.4 from calibration to Carbon-14 data. An even higher γ value of 0.569 was suggested for liquid flow in the main repository unit at Yucca Mountain, based on calibration to various field measurements (Bechtel SAIC Company, 2004b).

Table 2. List of sensitivity cases with different interface reductions. Also provided are the maximum fracture saturation values in grid elements adjacent to drift wall (upper half), simulated during the heating phase of the CNWRA experiment. For the cases using the active fracture model, the saturation of active fractures is displayed.

Case	**Interface Reduction Formulation**	**Reduction Factor**	**Reduction Applied only to Liquid Transfer ($R_{H,L}$ = 1)**	**Reduction Applied to Liquid and Heat Transfer ($R_{H,L}$ = R_L)**
			Case/Saturation	
1	Saturation-Dependent	$R_L = S_L$	Case 1a: 0.0	Case 1b: 0.10
2	Constant Factor	R_L = 0.1	Case 2a: 0.0	Case 2b: 0.09
3	Constant Factor	R_L = 0.01	Case 3a: 0.0	Case 3b: 0.18
4	Constant Factor	R_L = 0.002	Case 4a: 0.0	Case 4b: 0.19
5	Active Fracture Model	Eq. (2), γ = 0.3	Case 5a: 0.0	Case 5b: 0.21
6	Active Fracture Model	Eq. (2), γ = 0.569	Case 6a: 0.0	Case 6b: 0.31

Properties of the fractures and matrix continua have not been varied in this study, though we realize that they may have significant impact on the simulation results (Birkholzer et al., 2004). Some TH parameters, such as matrix permeability (affects matrix imbibition) or matrix thermal conductivity (affects heat exchange), directly affect the rate of liquid and heat transfer between fractures and matrix. However, we have limited our sensitivity study to analyzing various interface-reduction formulations, since differences between simulation cases are immediately linked to changes in fracture-matrix interaction. In contrast, variation in thermal-hydrological parameters will inevitably invoke other thermal-hydrological changes as well. Interested readers may be directed to Green et al. (2003) for an extensive sensitivity study regarding TH parameter variation.

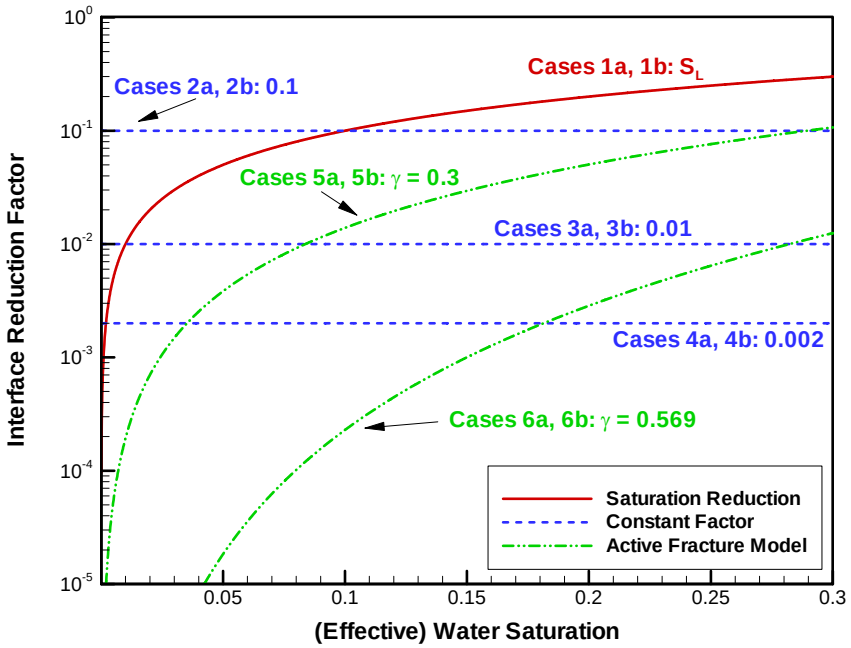

Figure 4. Interface reduction as a function of saturation. For cases using the active fracture model, we display the saturation of active fractures, $S_{Le,a}$.

4.2.2 Temperature Conditions Prior to Water Release

All sensitivity cases have identical temperature fields during the first 5 days of heating (no water release), since the same thermal-hydrological properties are used. Also, since the test cell is initially dry, no flow channeling in fractures and no related reduction in fracture-matrix interaction occurs. The simulated fracture and matrix temperatures are in local equilibrium. Figure 5 shows matrix temperature contours on the three-dimensional quarter-model after 5 days of heating, just prior to the onset of water release. The test cell has heated up considerably; the simulated temperature just above the crown of the drift in the center of the cell (x = 0 m, y = 0 m) is about 170°C, which compares well with the 175°C measured in the experiment (Green and Prikryl, 1998). The boiling point isotherm is located between 8 and 11 cm above the drift wall, depending on the axial location.

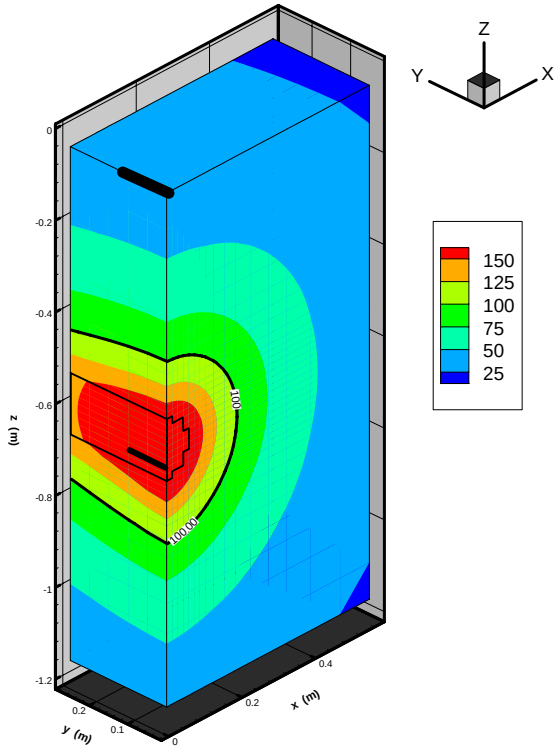

Figure 5. Temperature contours after 5 days of heating, just prior to the onset of water release. Black contour line shows 100°C-isotherm.

4.2.3 Model Results for Saturation-Dependent and Full Interface Case

We start our sensitivity evaluation with a detailed comparison of Case 1—using a saturation-dependent interface reduction—and Case F—assuming the full geometric interface between fractures and matrix. As shown in Figure 4, the saturation-dependent case features a moderate interface reduction compared to most of the other cases. We conducted two types of simulations for Case 1, one with interface reduction for liquid only (Case 1a: with $R_L = S_L$; $R_{H,L} = 1$), the second with interface reduction for liquid *and* heat (Case 1b: $R_L = R_{H,L} = S_L$). In our analysis below, we are mostly interested in (1) how the fast downward flow in fractures is affected by (and affects) the hot-fractured-rock region near the drift crown, and (2) whether liquid water can reach the drift vicinity despite above-boiling matrix temperatures.

The temporal evolution of simulated fracture and matrix temperatures, as well as fracture liquid saturation, are presented in Figures 6a and 6b, for a location in the fractured medium just above the drift crown in the center of the test cell. Figure 6c gives the distance of the boiling isotherm from the drift crown as a function of time. Note that the drift crown is about 0.52 m below the top of the test cell, where water infiltration begins after 5 days of heating. It is obvious

from the temperature plot that the water release of 1,000 mL/day tap water has a significant impact on the thermal conditions in the test cell. All simulation cases exhibit strong temperature drops during the infiltration period, the characteristics of which are dependent on the considered scenario.

Let us briefly discuss the relevance of the simulated matrix and fracture temperatures in a dual-continuum approach. The simulated matrix temperatures represent the thermal conditions in the bulk of the fractured porous medium. Temperature measurements in laboratory or field settings (e.g., from thermocouples) typically reveal matrix (or bulk) temperature. The simulated fracture temperature, on the other hand, represents the thermal conditions of the phases residing in the open conduits (for example the temperature of fast-flowing water). Such signals are often not detectable by sensors because their impact on temperature is local and short-lived. Matrix temperature is thus considered the measurable state variable.

In Case F, the matrix temperature at the drift crown continues to rise for a few days before the impact of infiltration becomes evident. With time progressing, temperature decreases steadily to about 108^{o}C at the end of the heating phase. More sudden responses in the matrix temperature occur in Cases 1a and 1b, with significant temperature drops soon after onset of water infiltration. As we will see later, these accelerated responses are caused by the fast movement of the liquid front down to the drift vicinity, a result of reduced imbibition. The sudden responses are followed by a relatively slow temperature decrease as time progresses; at the end of the heating phase, the matrix temperature in Case 1a (113^{o}C) and Case 1b (119^{o}C) is actually higher than in Case F.

The simulated fracture temperatures follow closely the matrix temperatures in Cases F and 1a, with some minor deviations at the end of the heating phase caused by the impact of nearby heat pipes. This is in strong contrast to the fracture temperature evolution observed in Case 1b, i.e., the simulation with reduced interface area for liquid *and* heat. The fracture temperature at the drift crown drops to the boiling point immediately after water release and remains at about 100^{o}C over the entire heating phase. This drop creates a strong disequilibrium between the matrix and the fracture temperatures, with matrix temperatures up to 60^{o}C higher at early heating stages. The immediate drop in the fracture temperature of Case 1b corresponds to the early arrival of liquid water at the drift crown (see Figure 6b). Thus, the simulation with reduced interface area for heat transfer allows for a situation in which fast-flowing water can penetrate the hot fractured rock and reach the drift crown, even while the temperature in adjacent matrix blocks is as high as 160^{o}C. At early times, the amount of water arriving at the drift crown is quite small, with saturation just

above residual. Later, the fracture saturation at the drift crown builds up, indicating that the impact of vaporization reduces with decreasing matrix temperatures. The maximum saturation of about 0.1 is reached between 70 and 130 days of heating. Seepage of water into the drift is possible under such conditions, and ultimately depends on the effectiveness of capillary forces at the rock-drift interface. In contrast, Cases F and 1a predict a fully effective vaporization barrier, with zero fracture saturation at the drift crown over the entire heating phase. Thus, the simulation cases assuming a full geometric interface area for heat transfer cannot explain why dripping of water was observed in the CNWRA experiment.

Note that Case 1b—with reduced thermal interaction between fracture and matrix—features the highest matrix temperatures over most of the heating phase, except for the early stages. Less cooling of the matrix blocks occurs, since the heat exchange with the cool water in the adjacent fractures is diminished. This effect can also be seen in the temporal evolution of the boiling point isotherm in Figure 6c. All simulation cases exhibit a fast early response, as the boiling zone recedes to less than half of its initial extent. At later stages, however, the boiling isotherm remains further away from the drift crown in Case 1b (about 4–5 cm at the end of the heating phase) compared to Cases F and 1a (about 2–3 cm at the end of the heating phase).

All simulation cases show a strong temperature decrease during the 10-day cooling phase, down to less than 40^{o}C at the end of the experiment (140 days). As temperature decreases below boiling, the differences between the simulation cases virtually disappear. Water saturation at the drift crown builds up immediately to maximum values of about 0.25. Thus, during the cooling phase, seepage of water into the drift is likely in all three cases. However, for analysis of thermal seepage (i.e., seepage into drifts despite above-boiling average temperatures in the near-drift fractured rock), we are only interested in the 125 days of simultaneous heating and water release.

Let us compare the three-dimensional flow patterns of water infiltrating down the fracture network towards the heated drift. Figure 7 shows fracture saturation contours at 10, 50, and 130 days after the onset of heating (i.e., after 5, 45, and 125 days of water release) for the upper part of the three-dimensional model domain. For comparison, the plots also include the location of the boiling isotherm determined from simulated matrix temperatures. All cases exhibit fast, focused, gravity-driven downward flow in response to water release at the top of the test cell. For example, after 5 days of infiltration, the liquid front has traveled most of the vertical distance between the release point and the drift. The colder water flowing in the fractures heats up on its way down; simultaneously, matrix temperature decreases in response to water arrival. As water encounters

above-boiling temperatures, the liquid front slows down. Vaporization and subsequent condensation lead to lateral flow diversion and drainage of water towards the bottom boundary. (Note that Green et al. (2003) report flow diversion around the drift in a zone approximately 15 cm wide, as concluded from mineral precipitation patterns observed after disassembling the test cell. This agrees favorably with the saturation distributions shown in Figure 7.) Saturations below the drift remain low because the flow region is sheltered from the downward infiltration.

The differences between the cases appear subtle, but are significant for thermal seepage. The most important difference is related to the location of the liquid front compared to the boiling isotherm. In Cases F and 1a, water does not penetrate into the boiling zone; the saturation front and the boiling front coincide. Enough energy is transmitted from the matrix to effectively vaporize the water as it arrives at the boiling front. In Case 1b, on the other hand, the simulated boiling front does not coincide with the simulated fracture saturation front. Here, water penetrates into the boiling region and reaches the drift, as the smaller interface area reduces the amount of energy available for boiling of fracture water. Water first arrives at the drift crown close to the center of the drift, vertically below the water release point. As time progresses, water accumulates over the entire length of the drift, including the end section. Since the capillary barrier is treated as fully effective, the accumulating water is diverted entirely around the drift.

Outside of the boiling region, Cases 1a and 1b have virtually identical saturation patterns. The reduction in heat transfer mostly affects the effectiveness of vaporization, because boiling requires considerably more energy than merely heating of water. There are, however, obvious differences compared to Case F regarding the flow patterns observed outside of the boiling zone. Since Case F assumes a full interface area for F-M liquid transfer, more water imbibes into the adjacent matrix compared to the other cases, which retards the early-time movement of the liquid front (see Figures 7a, 7b, and 7c at 10 days of heating). As a result, Case F features the least extended liquid front and the largest boiling region at 10 days of heating, when water release has just started. On the other hand, the same simulation case exhibits the smallest boiling region of all cases at the end of heating, because the interaction between the cool fracture water and the hot matrix is more effective. The temperature even drops below the boiling point near the unheated end of the drift, and water accumulates at the drift wall at 130 days of heating (which opens the possibility of seepage). However, Case F is not a likely scenario, because all temperature measurements in the CNWRA experiment suggest that the entire drift crown remains above boiling during the heating phase of the experiment (Green and Prikryl, 1998, 1999).

4.2.4 Model Results for Other Sensitivity Cases

In this section, we compare additional simulation cases using different interface reduction formulations. Each simulation applies the proposed approximate treatment for thermal F-M interaction, with interface reduction established for liquid *and* heat transfer. In addition to Case 1b—the saturation-dependent interface reduction which serves as a reference case—we chose two cases with constant reduction factors $R_L = R_{H,L} = 0.1$ (Case 2b) and $R_L = R_{H,L} = 0.002$ (Case 4b), as well as an active-fracture-model case with a γ value of 0.569 (Case 6b). In the last case, the interface reduction can be calculated from Equation (2). Note that Case 4b, with a constant factor of 0.002, utilizes approximately the same interface reduction for heat as the thermal seepage model used for predictive evaluation of thermally driven seepage at Yucca Mountain (Bechtel SAIC Company, 2004a).

Figures 8a, 8b, and 8c give the evolution of temperature and fracture liquid saturation close to the drift crown, as well as the location of the boiling isotherm above the drift crown (in the center of the test cell at x = 0 m and y = 0 m), for all four cases. We compare Cases 1b and 2b to evaluate the basic differences between a saturation-dependent and a constant-factor reduction. As shown in Figure 4, Case 2b features a moderate interface reduction similar to Case 1b. However, because of its linear correlation with local fracture saturation, the interface reduction in Case 1b is relatively strong at small saturation values, which may be typical of the situation when the tip of a liquid front penetrates into a boiling region of rock. In contrast, Case 2b uses a reduction factor of 0.1 regardless of the saturation value. Thus, we may expect a slower front propagation in Case 2b, because the downward migration of the tip of the moving front is more strongly affected by liquid and heat exchange with the matrix. As a matter of fact, water arrives at the drift crown approximately 25 days later in Case 2b compared to Case 1b, as evidenced by the slower temperature drop in Figure 8a and the retarded saturation buildup in Figure 8b. With time, the differences between the two cases decrease; at the end of the heating phase, the water saturations at the drift crown are almost identical at about 0.1 (which gives almost identical interface reduction factors). Note also that the matrix temperature response at the drift crown and the extent of the boiling zone are hardly affected by the moderate differences in interface reduction between Cases 1b and 2b.

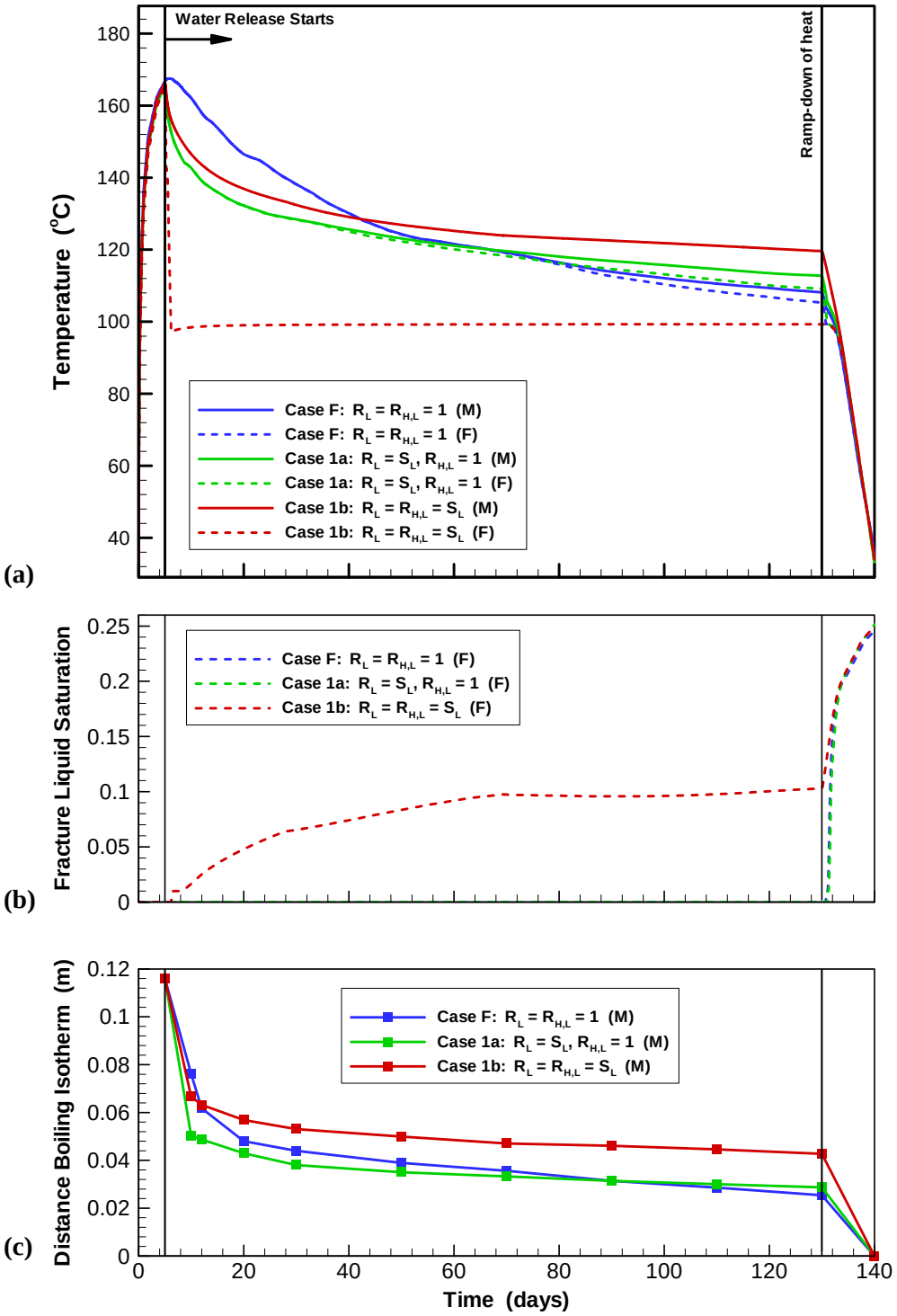

Figure 6. (a) Temperature and (b) saturation evolution just above the crown of the drift in the center of the test cell (x = 0 m, y = 0 m). The bottom graph (c) gives the evolution of the distance of the boiling isotherm above the drift crown, measured in the center of the test cell (x = 0 m, y = 0 m). The time axis scale is identical in all three graphs. “M” stand for matrix, “F” stands for fracture.

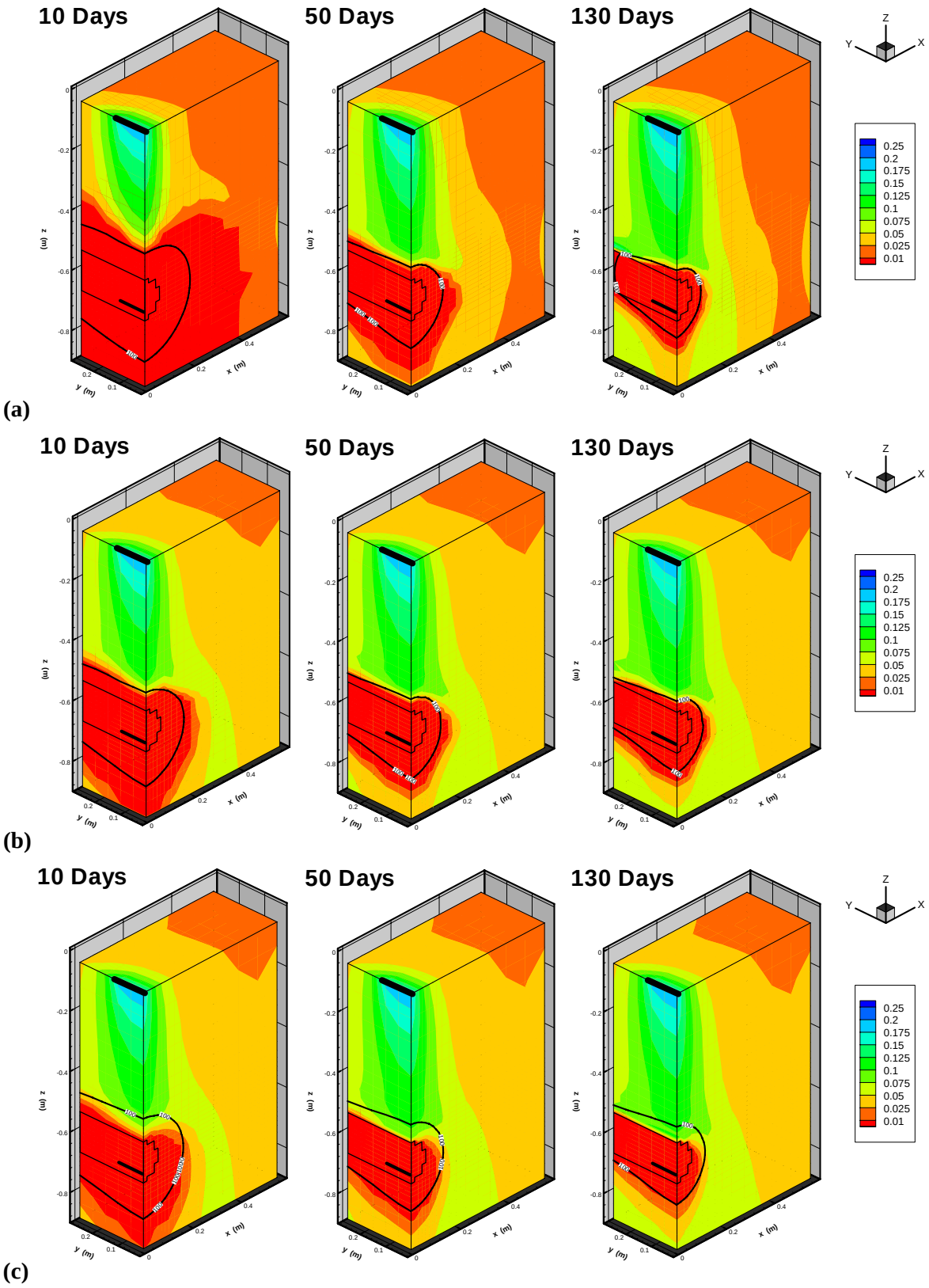

Figure 7. Fracture saturation contours after 10, 50, and 130 days of heating, for simulation runs (a) Case F, (b) Case 1a, and (c) Case 1b. Black contour line shows 100°C-isotherm.

Analyzing Cases 4b and 6b enables us to understand the impact of a rather extreme reduction in F-M interaction. In both cases, the water release at the top of the test cell leads to an immediate temperature drop and saturation increase in the fractures at the drift crown. The fracture saturations of about 0.19 (constant reduction factor of 0.002) and 0.31 (active fracture model) are higher than in the other two cases which increases the possibility of thermal seepage. An almost steady-state situation is established in the fractures soon after water arrives at the drift; temperature and saturation values are approximately constant over the remainder of the heating phase. Apparently the liquid front penetrates the hot fractured rock with only minor water losses due to boiling. The boiling zone would have to be much larger to noticeably retard or ultimately stop water penetration. Note that the evolution of matrix temperatures is affected by the strong interface reduction. Since the heat transfer between the hot matrix and the relatively cold liquid in the fractures is only a fraction of the more moderate interface reduction cases, cooling in the matrix is much slower (see Figure 8a and 8c). For example, the matrix temperature at the drift crown is still as high as 135 to 140^{o}C at the end of the heating phase in Cases 4b and 6b, compared to about 118^{o}C in Cases 1b and 2b. Similarly, the extent of the boiling zone above the drift crown is larger.

Figure 9 shows fracture saturation profiles along a vertical line between the drift crown and the top of the test cell at 10, 50, and 130 days of heating (at x = 0 m and y = 0 m). Differences between the four simulation cases are limited to the near-drift region; all saturation patterns are similar in the sub-boiling areas. (The exception is the simulation case featuring the active fracture model, which has higher saturation values over the entire vertical profile. However, these differences are not related to the treatment of F-M interaction. The saturation of active fractures, which is plotted in Figure 9, is larger compared to the other cases because the same amount of water needs to be conducted in fewer fractures.) The two extreme interface reduction cases (Cases 4b and 6b) show a considerable saturation buildup just above the drift wall, which is a typical observation in ambient unsaturated media when gravity-driven flow is diverted around a cavity (e.g., Philip et al., 1989; Birkholzer et al., 1999). Flow diversion requires a saturation increase at the crown to provide a pressure gradient driving water sideways and downwards. That such increases can be observed despite above-boiling temperature in the adjacent matrix blocks demonstrates that vaporization effects are not important for the downward flow of water in Cases 4b and 6b. The moderate interface reduction cases, on the other hand, show saturation decreasing close to the drift crown, suggesting that enough water vaporizes in the boiling region to suppress water accumulation from flow diversion effects.

For a quick comparison between all sensitivity cases, we have listed in Table 2 the maximum fracture saturations observed in any grid element along the upper half of the drift during the heating phase of the experiment. As pointed out before, the simulated fracture saturations provide a qualitative indicator for assessing whether the moisture conditions at the drift wall would allow for seepage into the opening or not. The saturation values in Table 2 reinforce the importance of interface-area reduction for heat transfer. All cases that assume the full geometric interface area for heat transfer end up with zero fracture saturation along the drift wall. In these cases, water is prevented from arriving at the drift crown by a fully efficient vaporization barrier. Seepage would not be possible under such conditions, which is in disagreement with the observation of precipitates in the drift in the CNWRA experiment (Green and Prikryl, 1999). In contrast, all cases that allow for heat transfer reduction exhibit water buildup at the drift crown despite above-boiling temperatures in the matrix, with maximum fracture saturations ranging from 0.09 in Case 1a to 0.31 in Case 6a. Locally, these values would be even higher if small-scale heterogeneities had been accounted for in the model. We may conclude that most, if not all sensitivity cases with interface reduction for heat transfer arrive at near-drift conditions that make thermal seepage likely. The more significant the interface reduction, the higher the fracture saturation values at the drift wall and the higher the potential for seepage.

It follows from the above discussion that the sensitivity cases featuring interface reduction for F-M heat transfer are generally better suited to represent the CNWRA test results than those assuming that heat is conducted over the full geometric area. But which of the interface reduction formulations for heat transfer is in best agreement with the experimental data? This is a difficult question to answer, for the following reasons. First, the literature on the CNWRA experiment (i.e., Green and Prikryl, 1998, 1999; Green et al., 2003) does not provide sufficient information to allow for a comprehensive comparative analysis using various data types, let alone to conduct a detailed model calibration. Second, all our sensitivity cases—ranging from moderate to rather extreme reduction in heat transfer—allow for penetration of water through the boiling region down to the drift crown, and thus can potentially lead to thermal seepage. Differences between these cases would be more obvious in a situation where the boiling isotherm was further away from the drift than the few-centimeters distance observed in the CNWRA experiment. Presumably, with a larger boiling region, water would not reach the drift crown in the more moderate sensitivity cases, while more extreme interface formulations would still allow for breaching of the vaporization barrier. Third, some cases exhibit only subtle differences in data that are easily measurable in experiments (such as matrix temperature), yet may differ

significantly in the potential for thermal seepage (as evidenced by the characteristics of saturation buildup at the drift crown which is hard to measure in experiments). For example, distinguishing between Cases 1b and 2b would be a challenging task, even if a comprehensive set of measured data were available from the CNWRA experiment. Cases 1b and 2b differ in the functional relationship, but feature an overall similar magnitude of interface reduction. We expect that the differences between cases with moderate versus strong interface reduction (e.g., Cases 1b and 2b versus Cases 4b and 6b) should be more obvious from experimental observations. Strong interface reduction results in less cooling of the matrix, because the infiltrating water effectively bypasses the matrix blocks. Thus, the measured temperature response in the matrix can be a good indicator for evaluating the magnitude of thermal F-M interaction.

4.3 Implications for Yucca Mountain Models

Our modeling analysis of the CNWRA experiment has demonstrated that the experimental observation of thermal seepage into a heated drift can be reproduced in the numerical simulations. All sensitivity cases that account for channelized flow in fractures and the related reduction in F-M heat transfer are capable of predicting TH conditions favorable for thermal seepage to occur. This result provides confidence that the conceptual model using an approximate treatment of thermal F-M interface reduction is adequate.

A similar conceptual approach for reducing heat transfer between fractures and matrix was chosen for the predictive analysis of thermal seepage during the heating phase of the Yucca Mountain repository. As mentioned before, the thermal seepage model (Bechtel SAIC Company, 2004a) utilized a constant reduction factor of about 0.002 for thermal interface reduction, similar to Case 4b studied in this paper. This rather extreme interface reduction most likely overestimates the impact of flow channeling on F-M interaction. Despite this extreme modeling choice, water was not able to penetrate far into the boiling regions and did not arrive at the drift walls during the first several hundreds of years after emplacement (Birkholzer et al., 2004).

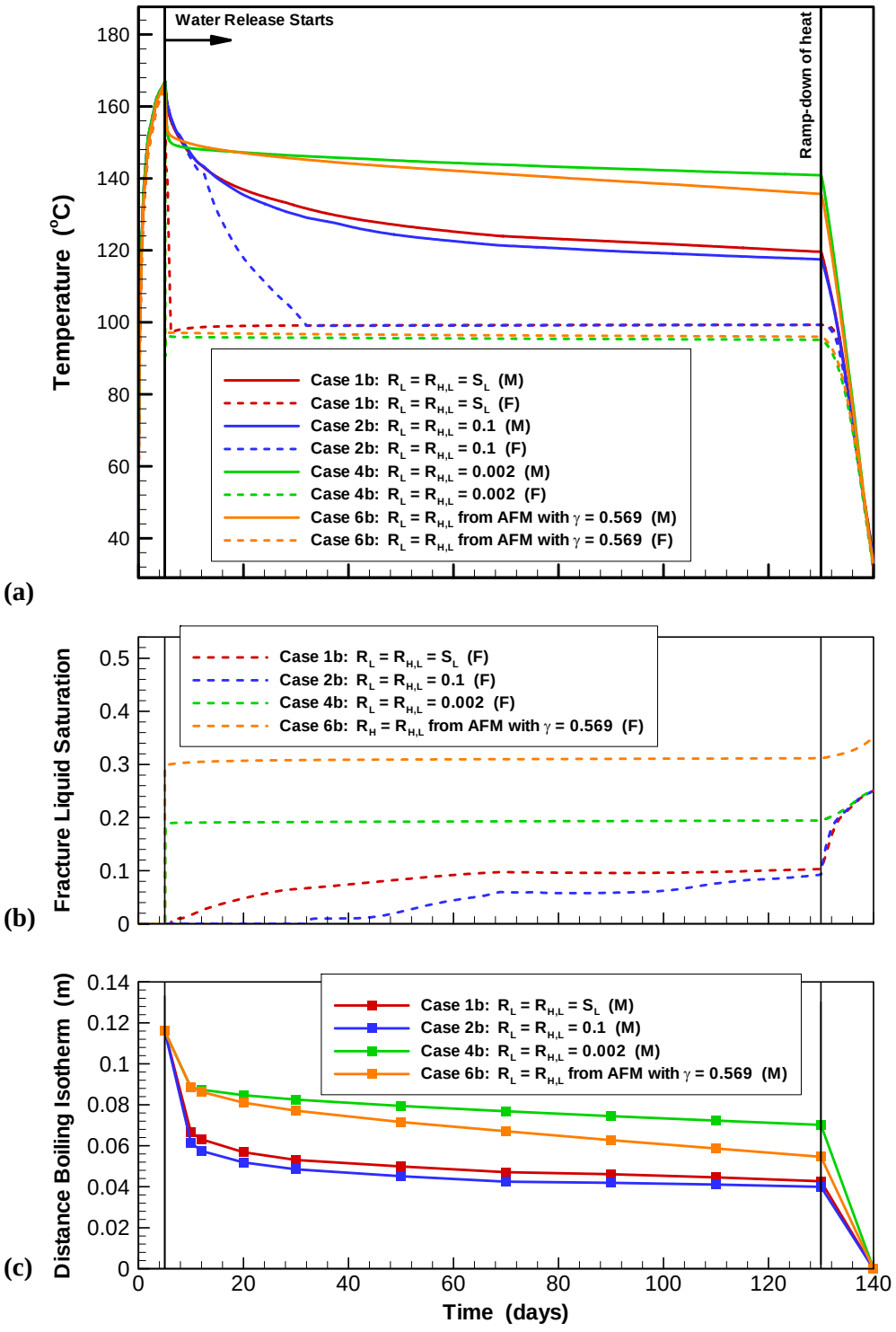

Figure 8. (a) Temperature and (b) saturation evolution just above the crown of the drift in the center of the test cell (x = 0 m, y = 0 m). The bottom graph (c) gives the evolution of the distance of the boiling isotherm above the drift crown, measured in the center of the test cell (x = 0 m, y = 0 m). Four simulation cases are compared, all with interface reduction for liquid and heat. The time axis scale is identical in all three graphs. "M" stand for matrix, "F" stands for fracture. For the case using the active fracture model (AFM), we display the saturation of active fractures, $S_{Le,a}$.

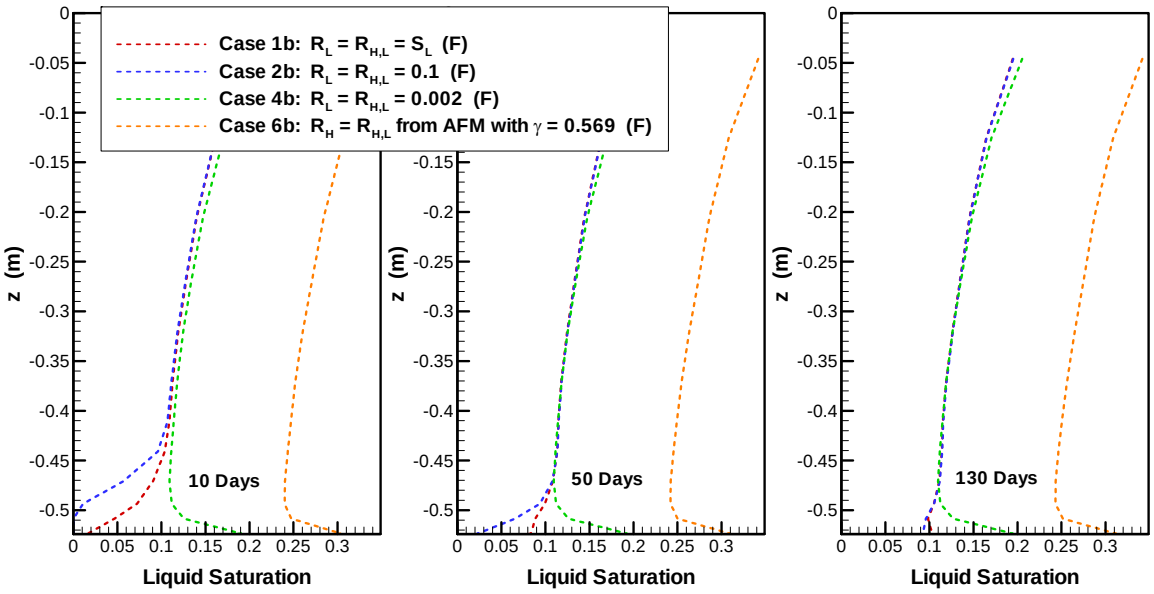

Figure 9. Fracture saturation along a vertical line above the heater crown (z = -0.525m), located in the center of the test cell (x = 0 m, y = 0 m). Four simulation cases are compared, all with interface reduction for liquid and heat. "F" stands for fracture. For the case using the active fracture model (AFM), we display the saturation of active fractures, $S_{Le,a}$.

We may conclude that the thermal seepage observations in the CNWRA experiment are not representative of the future TH conditions expected at Yucca Mountain. With respect to the possibility of water arrival at the drift crown, the most important differences between the CNWRA experiment and the Yucca Mountain conditions are related to (1) the size of the heated rock volume, in particular the extent of the boiling region, and (2) the intensity and the temporal evolution of downward flow above the heated drifts. In previous work, we have analyzed the predicted TH conditions relevant for thermal seepage at Yucca Mountain (Birkholzer et al., 2003). On average, the boiling region above a typical emplacement drift at Yucca Mountain is expected to cover more than 4 m of fractured rock over the first 500 years after emplacement. Conversely, in the CNWRA experiment, water release at the top gives rise to significant cooling of the test cell, and the location of the boiling isotherm recedes to a few centimeters above the drift crown. The smaller the boiling zone, the larger the possibility of channelized finger flow reaching the drift.

To evaluate Item (2) above, we compare the characteristics of the downward flow processes in the experiment to the Yucca Mountain setting. Since the average infiltration in the unsaturated rock is very small (between 5 and 10 mm/year), the main source of downward flow towards heated drifts at Yucca Mountain is from condensation of matrix pore water mobilized in the

boiling region. It follows that the intensity and evolution of thermal flux perturbation is directly linked to the intensity and evolution of heat. Accordingly, Birkholzer et al. (2003) report that the condensation-driven downward flux toward heated drifts at Yucca Mountain is largest during the first few hundred years after emplacement, corresponding to the period when the heat output of the radioactive waste is highest. During this time, the boiling zone in the fractured rock is large and effectively prevents water arrival at the drift, although the maximum downward fluxes of condensate (about 80 mm/yr for average conditions) exceed the natural infiltration by more than one order of magnitude. Later, when less heat emanates from the waste packages and the boiling zone becomes smaller, the thermal flux perturbation decreases accordingly, so that water arrival at the drift is also unlikely. This temporal correlation between flux intensity and extent of boiling zone at Yucca Mountain was shown to be very important in preventing thermal seepage (Birkholzer et al., 2003). Conversely, in the CNWRA experiment, downward flow is initiated by forced water release from the top of the test cell, maintained at a constant rate of 1,000 mL/day independent of thermal conditions. Using the footprint of the drift (0.15 m × 0.6 m) as a reasonable reference scale, this water release rate converts to a Darcy flux of over 4,000 mm/year, which is much larger than the condensate-driven downward flux expected at Yucca Mountain (Birkholzer et al., 2003).

We may conclude that the test conditions in the CNWRA experiment are extremely favorable for thermal seepage to occur, compared to the future situation at Yucca Mountain. In the CNWRA experiment, forced water release leads to intense gravity-driven downward flow that can easily penetrate through the small boiling region around the heated drift and lead to water accumulation at the drift crown.

5. Summary and Conclusions

We have conducted a sensitivity analysis studying the impact of fracture-matrix mass and heat transfer in hot fractured porous rock. Our motivation was to gain a better understanding of processes important for thermal seepage at the proposed geologic repository for radioactive waste at Yucca Mountain, Nevada. Thermal seepage is defined as seepage of water into emplacement drifts despite above-boiling rock temperatures in the adjacent fractured rock. The sensitivity study is performed using a laboratory heater test (CNWRA experiment) as a simulation example. It was shown in this heater test that fast downward flow in fractures could give rise to thermal seepage under certain conditions, thereby challenging earlier model predictions for Yucca Mountain in which thermal seepage was essentially ruled out.

The modeling framework for simulating the CNWRA experiment was adopted from simulation models established for the predictive evaluation of TH conditions and thermal seepage at Yucca Mountain. One relevant modeling element is the use of the dual-continuum approach, which treats the fractured rock as separate, interacting continua for fractures and matrix blocks, respectively. In unsaturated media, the magnitude of interaction is significantly dependent on the flow characteristics in the fractures. Channelized finger-type flow patterns, for example, lead to reduced interaction between the liquid phase in the fractures and the matrix, because only a small fraction of the entire fracture surface is available for mass and heat transfer. As a result, rapid channelized flow events are more likely to overcome the vaporization barrier formed by the hot rock and create conditions favorable for thermal seepage.

In our sensitivity analysis, we have varied the degree of F-M interaction in a dual-continuum model by applying different interface reduction approaches. We consider two main categories: (1) interface reduction for liquid transfer, but full geometric interface for heat transfer, (2) interface reduction for liquid *and* heat transfer. Conceptually, the latter category would involve a thermodynamic disequilibrium in the fracture continuum, because the penetration of cool water into a hot fracture network would give rise to local temperature differences between the liquid and the gas phase. Since most multiphase simulators are not suited for handling local disequilibrium conditions, we have developed an approximate interface reduction scheme, based on the notion that an accurate representation of the gas-phase temperature in the fractures is not necessary. For each of the above categories, we have applied various interface-reduction formulations available from the literature, specifically multiplication of the full geometric interface with a constant factor, multiplication with fracture liquid saturation, and multiplication

with factors derived from the active fracture model. For comparison, we have also studied a case using the full geometric interface without any reduction.

All simulation cases have indicated that the CNWRA experiment was operated at conditions favorable for thermal seepage. Most importantly, these conditions are (1) the rather small boiling region near the drift, and (2) the strong gravity-driven downward flow in response to forced water release from the top. These conditions are not representative of the future TH situation expected at Yucca Mountain, where the boiling region is much larger and where the downward flow characteristics are different in magnitude and temporal evolution. The potential for thermal seepage was evaluated for each simulation case, based on the simulated fracture saturation at the drift crown during the heating phase of the experiment. In other words, it was analyzed whether or not liquid water released from the top could reach the drift vicinity despite above-boiling temperatures in the rock matrix.

Our simulation results stress the importance of understanding and adequately simulating the degree of heat transfer between the matrix and the flowing water in fractures: All simulation cases featuring interface reduction for heat transfer—ranging from moderate to rather extreme reduction—exhibit early and consistent arrival of water at the drift crown, even though the matrix temperatures show no clear indication of such events and remain above boiling throughout the heating phase. Thermal seepage is possible under these conditions, which is consistent with the experimental findings. In contrast, if interface reduction is not considered at all or is only applied to liquid exchange processes, the saturation front and the boiling isotherm coincide, and water is prevented from arriving at the drift crown by a fully efficient vaporization barrier. We conclude that the sensitivity cases featuring interface reduction for F-M heat transfer represent the CNWRA test results much better than those assuming that heat is conducted over the full geometric area.

Attempts to identify the interface reduction formulation best suited to describe the reduced heat transfer in the CNWRA experiment failed. This is in part a result of the test geometry, because the region of above-boiling rock temperature was too small to bring out clear differences between the simulation cases. With a more extended boiling region, water would not reach the drift crown in the more moderate sensitivity cases, while more extreme interface formulations would still allow for breaching of the vaporization barrier. Future work should be directed at conducting and interpreting large-scale *in situ* experiments, ideally with an above-boiling rock

region of a few meters extent. Such a test should be operated at different levels of water release to create conditions more or less favorable for thermal seepage.

Our simulation results have also indicated that, under well-controlled thermal conditions, the temperature response in the matrix to water release from the top could be a good indicator for the degree of thermal F-M interaction. Cases with strongly reduced interface area show typically less temperature decrease in the matrix, because there is less interaction with the cool water flowing in the fractures. This effect could be important in field settings, where measurements of matrix temperature are relatively simple and inexpensive.

Acknowledgment

This work was supported by the Director, Office of Civilian Radioactive Waste Management, U.S. Department of Energy, through Memorandum Purchase Order QA-B004220RB3X between Bechtel SAIC Company, LLC, and the Ernest Orlando Lawrence Berkeley National Laboratory (Berkeley Lab). The support is provided to Berkeley Lab through the U.S. Department of Energy Contract No. DE-AC03-76SF00098. Review and comments of Stefan Finsterle and Dan Hawkes from Berkeley Lab are gratefully appreciated. We also would like to acknowledge the helpful comments of ?? anonymous reviewers.

References

Altman, S.J., B.W. Arnold, R.W. Barnard, G.E. Barr, C.K. Ho, S.A. McKenna, and R.R. Eaton, Flow calculations for Yucca Mountain groundwater travel time (GWTT-95), SAND96-0819, Albuquerque, New Mexico, Sandia National Laboratories, 1996.

Bandurraga, T.M., and G. S. Bodvarsson, Calibrating hydrogeologic parameters for the 3-D site-scale unsaturated model of Yucca Mountain, Nevada, *Journal of Contaminant Hydrology*, 38(1-3), 47-56, 1999.

Birkholzer, J.T., G. Li, C.-F. Tsang, and Y.W. Tsang, Modeling studies and analysis of seepage into drifts at Yucca Mountain, *Journal of Contaminant Hydrology*, 38(1-3), 349-384, 1999.

Birkholzer, J.T., and Y.W. Tsang, Modeling the thermal-hydrologic processes in a large-scale underground heater test in partially saturated fractured tuff, *Water Resources Research*, 36(6), 1431-1447, 2000.

Birkholzer, J.T., Penetration of liquid fingers into superheated fractured rock, *Water Resources Research*, 39(4), 9-1 through 9-21, 2003.

Birkholzer, J.T., and C.K. Ho, A probabilistic analysis of episodic preferential flow into superheated fractured rock, *Journal of Hydrology*, 284, 151-173, 2003.

Birkholzer, J.T., S. Mukhopadhyay, and Y.W. Tsang, The impact of preferential flow on the vaporization barrier above waste emplacement drifts at Yucca Mountain, Nevada, *Journal of Nuclear Technology*, 148, 138-150, 2003.

Birkholzer, J.T., S. Mukhopadhyay, and Y.W. Tsang, Modeling seepage into heated waste emplacement tunnels in unsaturated fractured rock, *Vadose Zone Journal*, 3, 819-836, 2004.

Bechtel SAIC Company, Drift-scale coupled processes (DST and TH Seepage) models, MDL-NBS-HS-000015 REV 01, Las Vegas, Nevada, 2004a.

Bechtel SAIC Company, Calibrated properties model, MDL-NBS-HS-000003 REV 02, Las Vegas, Nevada, 2004b.

Buscheck, T.A., and J.J. Nitao, The analysis of repository-heat-driven hydrothermal flow at Yucca Mountain, in Proceedings of the 4th Annual High-Level Radioactive Waste Management Conference, Las Vegas, NV, 449-471, 1993.

Buscheck, T.A., N.D. Rosenberg, J. Gansemer, and Y. Sun, Thermohydrologic behavior at an underground nuclear waste repository, *Water Resources Research*, 38(3), 1-19, 2002.

Doughty, C., Investigation of conceptual and numerical approaches for evaluating moisture, gas, chemical, and heat transport in fractured unsaturated rock, *Journal of Contaminant Hydrology*, 38(1-3), 69-106, 1999.

Finsterle, S., C.F. Ahlers, R.C. Trautz, and P.J. Cook, Inverse and predictive modeling of seepage into underground openings, *Journal of Contaminant Hydrology*, 62-63, 89-109, 2003.

Ghezzehei, T.A., R.C. Trautz, S. Finsterle, P.J. Cook, and C.F. Ahlers, Modeling coupled evaporation and seepage in ventilated cavities, *Vadose Zone Journal*, 3, 806-8818, 2004.

Green, R.T., and J.D. Prikryl, Penetration of the boiling isotherm by flow down a fracture, in Proceedings of the Third International Conference on Multi-Phase Flow, ICMF'98, Lyon, France, June 8-12, 1998.

Green, R.T., and J.D. Prikryl, Formation of a dry-out zone around a heat source in a fractured porous medium, in Proceedings of the Second International Symposium on Two-Phase Flow Modeling and Experimentation, Pisa, Italy, May 23-26, 1999.

Green, R.T., S. Painter, B. Fratesi, C. Manepally, and G. Walter, Status report for multiphase flow simulation, Center for Nuclear Waste Regulatory Analysis, San Antonio, Texas, 2003.

Haukwa, C.B., Y.-S. Wu, and G.S. Bodvarsson, Thermal loading studies using the Yucca Mountain unsaturated zone model, *Journal of Contaminant Hydrology*, 38 (1-3), 217-255, 1999.

Haukwa, C.B., Y.W. Tsang, Y.-S. Wu, and G.S. Bodvarsson, Effect of heterogeneity on the potential for liquid seepage into heated emplacement drifts of the potential repository, *Journal of Contaminant Hydrology*, 62-63, 509-527, 2003.

Ho, C.K., Models of fracture-matrix interactions during multiphase heat and mass flow in unsaturated fractured porous media, in Proceedings of the Sixth Symposium on Multi-Phase Transport in Porous Media, Dallas, Texas, November 16-21, 1997.

Liu, H.H., C. Doughty, and G.S. Bodvarsson, An active fracture model for unsaturated flow and transport in fracture rocks, *Water Resources Research*, 34(10), 2633-2646, 1998.

Liu, H.H., G. Zhang, and G.S. Bodvarsson, The active fracture model: its relation to fractal flow patterns and an evaluation using field observationss, *Vadose Zone Journal*, 2, 259-269, 2003.

Mukhophadhyay, S., and Y.W. Tsang, Understanding the anomalous temperature data from the Large Block Test at Yucca Mountain, Nevada, *Water Resources Research*, 38(10), 28-1 through 28-12, 2002.

Mukhophadhyay, S., and Y.W. Tsang, Uncertainties in coupled thermal-hydrological processes associated with the Drift Scale Test at Yucca Mountain, Nevada, *Journal of Contaminant Hydrology,* 62-63, 595-612, 2003.

Pinder, G.F., P.S. Huyakorn, and E.A. Sudicky, Simulation of flow and transport in fractured porous media, in *Flow and Contaminant Transport in Fractured Rock,* Academic, San Diego, California, 1993.

Philip, J.R., J.H. Knight, and R.T. Waechter, Unsaturated Seepage and Subterranean Holes: Conspectus, and Exclusion Problem for Circular Cylindrical Cavities, *Water Resources Research,* 25(1), 16-28, 1989.

Phillips, O.M., Infiltration of a liquid finger down a fracture into superheated rock, *Water Resources Research,* 32(6), 1665-1670, 1996.

Pruess, K., GMINC—A mesh generator for flow simulations in fractured reservoirs, LBL-15227 Berkeley, California, Lawrence Berkeley National Laboratory, 1993.

Pruess, K., TOUGH User's Guide, NUREG/CR-4645, Washington, D.C., U.S. Nuclear Regulatory Commission, 1987.

Pruess, K., and Y.W. Tsang, Thermal modeling for a potential high-level nuclear waste repository at Yucca Mountain, Nevada, LBL-33597 UC-200, Berkeley, California, Lawrence Berkeley National Laboratory, 1993.

Pruess, K., and Y.W. Tsang, Modeling of strongly heat-driven flow processes at a potential high-level nuclear waste repository at Yucca Mountain, Nevada, LBL-35381 UC-600, Berkeley, California, Lawrence Berkeley National Laboratory, 1994.

Pruess, K., J.S.Y. Wang, and Y.W. Tsang, On thermohydrologic conditions near high-level nuclear wastes emplaced in partially saturated fractured tuff, 1, Simulation studies with explicit consideration of fracture effects, *Water Resources Research,* 26(6), 1235-1248, 1990a.

Pruess, K., J.S.Y. Wang, and Y.W. Tsang, On thermo-hydrologic conditions near high-level nuclear wastes emplaced in partially saturated fractured tuff, 2. effective continuum approximation, *Water Resources Research,* 26(6), 1249-1261, 1990b.

Pruess, K., C. Oldenburg, and G. Moridis, TOUGH2 User's Guide, Version 2.0, LBNL-43134, Berkeley, California, Lawrence Berkeley National Laboratory, 1999.

Ramspott, L.D., The constructive use of heat in an unsaturated tuff repository, in Proceedings of the 2nd Annual High-Level Radioactive Waste Management Conference, Las Vegas, NV, 1991.

Thoma, S.G., P. Gallegos, and D.M. Smith, Impact of fracture coating on fracture/matrix flow interactions in unsaturated media, *Water Resources Research*, 28(5), 1357-1367, 1992.

Tsang, Y.W., and J.T. Birkholzer, Predictions and observations of the thermal-hydrologic conditions in the Single Heater Test, *Journal of Contaminant Hydrology*, 38(1-3), 395-426, 1999.

van Genuchten, M.T., A closed-form equation for predicting the hydraulic conductivity of unsaturated soils, *Soil Science Society of America Journal*, 44, 892-898, 1980.

Wilder, D.G., Alternative strategies—A means for saving money and time on the Yucca Mountain project, in Proceedings of the 4th Annual High-Level Radioactive Waste Management Conference, Las Vegas, NV, 1993.

Appendix

The approximate approach for thermal F-M interaction introduced in Section 2.3 ignores the local disequilibrium between liquid- and gas-phase temperatures that can evolve as a result of channelized water flow in the fracture continuum. To allow application of equilibrium models, the liquid-phase temperature in the fractures is used to describe the thermal state in both phases. This approximate treatment misrepresents the gas-phase temperature, introducing an error in the numerical simulation. The impact of this error is evaluated below for the TH conditions observed in the CNWRA experiment. We study a situation similar to the schematic in Figure 2, where liquid fingers penetrate into a hot fracture-rock system. The liquid is at a temperature close to the boiling point of water at prevailing pressure ($T_{F,L} \approx 100^{o}$C), while the matrix temperature is significantly higher (compare Figures 6a and 8a). The gas phase in the fractures is similar to the matrix temperature ($T_{F,G} \approx T_M$), but in the approximate scheme is described by the local temperature of the liquid phase. Thus, the error in gas-phase temperature equals the difference between T_M and the boiling temperature of water.

As a first criterion, we calculate the relative error in energy storage. The error in the gas-phase temperature leads to an energy discrepancy in the fracture. This discrepancy should be small compared to the heat stored in the other phases present in the system, i.e., the solid phase and the water phase.

For a given fracture volume V_F and given gas saturation ($1 - S_L$), the energy discrepancy E_G in the gas phase can be calculated as

$$E_G = V_F \left(1 - S_L\right) \rho_G C_G \left(T_M - 100^o C\right), \qquad \text{(A1)}$$

where ρ_G is gas density and C_G is gas specific heat. The fracture volume is 4×10^{-4} m^3 for a 1-m^2 fracture with an aperture of 0.4 mm (the aperture value estimated for the CNWRA experiment). We may assume that the gas phase in the fracture consists entirely of vapor and insert the thermophysical properties of vapor at 100^{o}C and 1 bar ($\rho_G \approx 0.6$ kg/m^3; $C_G \approx 2.02$ kJ/kg-K). Reasonable values of liquid saturation and matrix temperature for the CNWRA experiment can be extracted from Figures 6 and 8. With a liquid saturation of 0.05 and a matrix temperature of 160^{o}C (representative of the test conditions just after water release), the resulting energy discrepancy is 0.03 kJ. (Similar results would be obtained when the gas phase comprises an air-

vapor mix or pure air. For example, using $\rho_G \approx 0.9$ kg/m^3 and $C_G \approx 1.0$ kJ/kg-K of pure air at 370 K, the resulting energy discrepancy would be 0.02 kJ.)

First compare this energy discrepancy with the energy stored in the solid phase (i.e., the matrix). We can calculate the matrix volume V_M associated with the fracture volume V_F from the fracture volume fraction (0.016 in Table 1), giving $V_M = (1\text{-}0.016)V_F/0.016 = 0.0246$ m^3. If we ignore the energy contributions from gas or liquid phases stored in matrix pores, the energy E_M contained in V_M is

$$E_M = V_M (1-\phi_M)\rho_M C_M T_M \ , \tag{A2}$$

where ϕ_M is matrix porosity, ρ_M is grain density, and C_M is grain heat capacity (Table 1). For a matrix temperature of 160^{o}C, the resulting energy amounts to 2645 kJ. Compared to this value, the energy discrepancy from misrepresentation of gas phase temperature is negligible.

More stringent is a comparison with the heat stored in the fracture water, which can be calculated as

$$E_F = V_F S_L \rho_L C_L T_{F,L} \ . \tag{A3}$$

Here, ρ_L is liquid density and C_L is liquid specific heat ($\rho_L \approx 958$ kg/m^3 and $C_L \approx 4.19$ kJ/kg-K at 100^{o}C and 1 bar). The resulting energy contained in the water is 8 kJ, which is still much larger than the energy discrepancy E_G from misrepresentation of the gas-phase temperature.

The second criterion is related to the heat transfer between the two phases present in the fracture. With the gas-phase temperature much higher than the liquid temperature, heat would be conducted between the two phases, which is neglected in the approximate approach for F-M interaction. We compare the importance of this interphase heat conduction with the heat transferred from the matrix to the water in the fracture, to evaluate whether the liquid front movement could possibly be affected. Heat transfer from the matrix can be directly calculated from Equation (3), using the property values given in Table 1 and assuming a saturation-dependent interface reduction. Adopting the above specifications, the fracture area considered is 1 m^2, water saturation is 0.05, and the temperature difference between the matrix and the water in

the fracture is 60°C. We arrive at a heat flux of 240 W when using the thermal-conductivity value for a dry matrix, and at 480 W when using the wet thermal-conductivity value.

Heat conduction between the gas phase and the water phase can be estimated from the following equation:

$$F_{GL} = A_{GL}\lambda_G \frac{\left(T_M - 100^O C\right)}{d} . \qquad \text{(A4)}$$

Here, A_{GL} is the interface area for heat conduction, given by the fracture aperture times the perimeter of the wetting front, λ_G is gas phase thermal conductivity, and d is a representative distance between the gas phase and the liquid phase. We assume a simple wetting-front geometry consistent with a liquid saturation of 0.05. Conservatively, we use relatively large interface area, e.g., by assuming five individual liquid fingers of 0.01 m width each and 1 m vertical length, which results in $A_{GL} = 4 \times 10^{-3}$ m^2. We may set d = 0.005 m, half the width of the liquid finger. Using a thermal conductivity of 0.03 W/kg-K for the gas phase, the interphase heat flux is between 1 and 2 W, less than 1% of the conductive flux from the matrix. Thus, the conductive heat flux between gas and liquid phases in the fractures can be safely neglected.

We can conclude that the proposed approximate treatment of F-M interaction in Section 2.3 is reasonably accurate for the conditions considered in the CNWRA experiment.